Potential and spin-exchange interaction between Anderson impurities in graphene

M. Agarwal and E. G. Mishchenko
Department of Physics and Astronomy, University of Utah, Salt Lake City, Utah 84112, USA

(Received 2 March 2018; revised manuscript received 4 February 2019; published 27 February 2019)

The effective interaction between resonant magnetic Anderson impurities in graphene, mediated by conduction electrons, is studied as a function of the strength of the on-site energy level of the impurities and the amplitude of coupling to conduction electrons. The sign and character of the interaction depend on whether the impurities reside on the same or opposite sublattices. For the same (opposite) sublattice, the potential interaction is attractive (repulsive) in the weak coupling limit with $1/R^3$ dependence on the distance; the interaction reverses sign and becomes repulsive (attractive) in the strong coupling limit and displays $1/R$ behavior. The spin-exchange coupling is ferromagnetic (antiferromagnetic) at both large and small distances, but reverses sign and becomes antiferromagnetic (ferromagnetic) for intermediate distances. For opposite sublattices, the effective spin-exchange coupling is resonantly enhanced at distances where the energy levels cross the Dirac points.

DOI: 10.1103/PhysRevB.99.085439

I. INTRODUCTION

Doping novel two-dimensional materials with magnetic atoms is one of the active areas of research where the ultimate objective is to design systems with the desired magnetic properties. To better exploit an emerging magnetism in such doped materials, it is important to understand how magnetic impurities [1–9] interact with each other.

Impurities in conventional three-dimensional metals induce famous charge (Friedel) and spin density (Ruderman-Kittel-Kasuya-Yosida) oscillations of the conduction electron density, $\propto \cos(2k_F R)/(k_F R)^3$, in the long-distance limit. In conventional two-dimensional electronic systems [10,11], the amplitude of these oscillations decays inversely proportional to the square of the distance. One exception is graphene, a two-dimensional material known for its remarkable electronic properties and potential for applications [12–16]. Density oscillations in graphene in both intrinsic (undoped) and extrinsic (doped) limit decay as [17] $\propto 1/R^3$, much like in three-dimensional systems. The RKKY interaction between magnetic impurities in graphene has also been studied extensively [18–25]. The sign of the RKKY interaction for a bipartite lattice of intrinsic graphene at half-filling is dictated by the particle-hole symmetry and is antiferromagnetic (ferromagnetic) when the impurities reside on different (same) sublattices. This is found at all length scales, with the exception of graphene nanoribbons, where presence of zero-energy modes complicates the picture [25–28]. For example, RKKY exchange coupling between spins of impurities located on the same sublattice has the following oscillatory behavior [21]: $J_{AA} \propto -\{1+\cos[(\mathbf{K}-\mathbf{K}')\cdot\mathbf{R}]\}/R^3$, where $\mathbf{K}$ and $\mathbf{K}'$ are the positions of two Dirac valleys in the reciprocal lattice. The coupling between spins on different sublattices, J_{AB}, has a similar oscillatory pattern, but the negative sign and the amplitude that is three times larger than in the AA case.

The above-referenced studies considered interactions of impurity atoms with the host material perturbatively. On the other hand, some adatoms (such as hydrogen) are better described by the Anderson model of a localized orbital hybridized with a conduction band of a host material. Such a model allows for a strong coupling of the localized orbital to conduction electrons. In the present paper, we consider two Anderson impurities with a low energy orbital ϵ_o hybridized with the π-band of graphene with some amplitude γ. We further assume that the orbital is below the Fermi energy (Dirac point) of undoped graphene, $\epsilon_o < 0$, and that the Coulomb on-site energy U_C is large enough, $\epsilon_o + U_C > 0$, so there is always an uncompensated spin $1/2$ associated with the impurity. Such assumptions work well for hydrogen adatoms, which have energy levels close to the Dirac point of graphene [29]. It is known that chemisorption of hydrogen atoms on graphene can indeed induce magnetic moments [30].

Magnetic applications of graphene would benefit from the ability to control magnetic moments. This, in turn, requires knowledge of the magnitude and sign of the effective exchange coupling between dopants. Of particular interest is the behavior of resonant Anderson impurities, where the orbital ϵ_o resides close to the Dirac points [17,29]. This results in the enhanced scattering of conduction electrons off the impurity [17].

It is instructive to begin our analysis of the Anderson-type impurities with a discussion of potential impurities. Recent studies [31–34] of impurity-impurity interaction in the case of substitution impurities with an on-site potential U have obtained an analytical expression exact in U [35–37]. In particular, in the large U limit, interaction between impurities on the same sublattice is long range, $\propto 1/R$ (up to logarithmic factors), and is repulsive, in contrast to the weak U limit, where it decays as $1/R^3$ and is attractive. The interaction between impurities residing on opposite sublattices similarly reverses sign and changes behavior when the strength U varies. Effectively, the Anderson impurity maps on the potential impurity model if one replaces the on-site potential strength U with the energy-dependent coupling parameter $\gamma(E)$, $U \to \gamma(E) = \frac{\gamma^2}{E-\epsilon_o}$. The weak potential impurity limit, analogous to the Anderson model with small $\gamma(E)$, maps onto

the case of a large on-site energy ϵ_o and/or small amplitude γ such that $\gamma(E) = -\gamma^2/\epsilon_o$ is an energy-independent constant for most energies except $E \sim \epsilon_o$. As a result, the interaction of both types of impurities depends on the coordinate in a similar fashion, $\propto U^2/R^3 \to \gamma^4/\epsilon_o^2 R^3$. With decreasing the distance R between the impurities, the strong coupling limit is achieved when the on-site energy U becomes of the order of v/R. In this strong coupling limit, the effective interaction energy is given by this very ratio v/R, since once U drops out of the picture, there is only one remaining low-energy scale in the system. The sign of the interaction is repulsive (attractive) for impurities belonging to the same (different) sublattices. Below, in Sec. III, we confirm that Anderson impurities in the resonant coupling regime demonstrate a similar R dependence.

We then investigate the effective spin-spin-exchange coupling $J_{\rm eff}(\mathbf{R})$ between two Anderson impurities in graphene and compare it with our recent results for substitutional potential impurities [37]. We limit our analysis to the lowest (second) order in the coupling J between the localized spins and conduction electrons but explore a broad range of the parameters ϵ_o and γ. The case of weak Anderson impurities yields $J_{\rm eff}(\mathbf{R}) \propto J^2/R^3$, similar to effective spin coupling in the potential impurity case. Both the sign and the $1/R^3$ dependence of the exchange coupling constants are consistent with the results in the existing literature, calculated within the conventional RKKY approach [21,25,31]. We then explore how $J_{\rm eff}(\mathbf{R})$ behaves in the strong coupling limit. In our recent work [37], we have shown that the effective spin-exchange coupling between substitutional magnetic impurities can become resonantly enhanced at a specific distance where an impurity level crosses the Dirac point. We find similar enhancement for Anderson impurities for sufficiently large couplings γ^2/ϵ_o.

We also consider a case where impurities are of different types, namely an Anderson impurity interacting with a substitutional impurity. A rather interesting situation arises where one of the impurities is weak whereas the second impurity is strong or resonant. This situation cannot be reduced to the perturbative RKKY-type calculations. In this situation, both the potential part of the interaction and its spin-spin-exchange part depends on the distance between the impurities as $1/R^2$.

This paper is organized as follows: In Sec. II, we discuss the energy levels of two Anderson impurities. In Secs. III and IV, we derive general expressions for the potential interaction and the spin-exchange coupling between the impurities, respectively, and consider the limiting case of $\epsilon_o = 0$. In Sec. V, we derive expressions for the potential interaction between an Anderson impurity and a substitutional impurity. We also looked at the spin-spin exchange coupling for a weak Anderson impurity and a strong potential impurity.

II. ENERGY LEVELS OF A TWO-IMPURITY SYSTEM

We consider the tight-binding model of π electrons in graphene interacting with two Anderson impurities located at $\mathbf{r}_1 = 0$ and $\mathbf{r}_2 = \mathbf{R}$. To calculate the interaction between the impurities, we first determine the energy spectrum of the system. The Hamiltonian of the system consists of the kinetic energy of electrons, the on-site impurity energy level ϵ_o, and a coupling term describing hybridization of conduction band with the impurity states with amplitude γ,

$$H_a = t\sum_{\mathbf{r}}\sum_{i=1,2,3}\hat{\psi}^\dagger(\mathbf{r})\hat{\psi}(\mathbf{r}+\mathbf{a}_i) + \epsilon_o\sum_{j=1,2}\hat{d}^\dagger(\mathbf{r}_j)\hat{d}(\mathbf{r}_j) + \gamma\sum_{j=1,2}[\hat{d}^\dagger(\mathbf{r}_j)\hat{\psi}(\mathbf{r}_j) + \hat{\psi}^\dagger(\mathbf{r}_j)\hat{d}(\mathbf{r}_j)]. \quad (1)$$

Here t is the hopping integral, $\hat{\psi}$ is electron operator of conduction electrons; $\hat{\psi}(\mathbf{r}) = \hat{a}(\mathbf{r})$ when $\mathbf{r}$ belongs to sublattice A, $\hat{\psi}(\mathbf{r}) = \hat{b}(\mathbf{r})$ when it belongs to sublattice B, and $\hat{d}$ is the operator of the localized impurity states. The index j enumerates the impurities. Using the Fourier representation for the electron operators, $\hat{\psi}(\mathbf{r}) = \sqrt{\frac{2}{N}}\sum_{\mathbf{k}}\hat{\psi}(\mathbf{k})e^{i\mathbf{k}\cdot\mathbf{r}-iEt}$, we obtain from the equation of motion, $i\partial\hat{\psi}(\mathbf{r},t)/\partial t = [\hat{\psi}(\mathbf{r},t), H]$, the following system of coupled equations (for the AB impurity configuration):

$$E\hat{a}(\mathbf{k}) = t(\mathbf{k})\hat{b}(\mathbf{k}) + \sqrt{\frac{2}{N}}\gamma\hat{d}(0), \quad (2)$$

$$E\hat{b}(\mathbf{k}) = t^*(\mathbf{k})\hat{a}(\mathbf{k}) + \sqrt{\frac{2}{N}}\gamma e^{-i\mathbf{k}\cdot\mathbf{R}}\hat{d}(\mathbf{R}), \quad (3)$$

$$E\hat{d}(0) = \epsilon_o\hat{d}(0) + \sqrt{\frac{2}{N}}\gamma\sum_{\mathbf{k}}\hat{a}(\mathbf{k}), \quad (4)$$

$$E\hat{d}(\mathbf{R}) = \epsilon_o\hat{d}(\mathbf{R}) + \sqrt{\frac{2}{N}}\gamma\sum_{\mathbf{k}}\hat{b}(\mathbf{k})e^{i\mathbf{k}\cdot\mathbf{R}}, \quad (5)$$

where $t(\mathbf{k}) = t\sum_i e^{i\mathbf{k}\cdot\boldsymbol{a}_i}$ and N is the total number of carbon atoms. Eliminating $\hat{d}(0)$ and $\hat{d}(\mathbf{R})$ gives

$$(E-\epsilon_o)[E\hat{a}(\mathbf{k}) - t(\mathbf{k})\hat{b}(\mathbf{k})] = \frac{2\gamma^2}{N}\sum_{\mathbf{k}'}\hat{a}(\mathbf{k}'),$$

$$(E-\epsilon_o)[E\hat{b}(\mathbf{k}) - t^*(\mathbf{k})\hat{a}(\mathbf{k})] = \frac{2\gamma^2}{N}\sum_{\mathbf{k}'}\hat{b}(\mathbf{k}')e^{i(\mathbf{k}'-\mathbf{k})\cdot\mathbf{R}}.$$

Solving the above two equations yields the equation for the localized impurity energy levels,

$$\left[1-\gamma^2\sum_{\mathbf{k}}A(\mathbf{k},0)\right]^2 = \gamma^4\sum_{\mathbf{k}}B(\mathbf{k},\mathbf{R})\sum_{\mathbf{k}'}B(-\mathbf{k}',\mathbf{R}), \quad (6)$$

where

$$\begin{Bmatrix}A(\mathbf{k},\mathbf{R})\\ B(\mathbf{k},\mathbf{R})\end{Bmatrix} = \frac{2e^{-i\mathbf{k}\cdot\mathbf{R}}}{N(E^2-|t(\mathbf{k})|^2)(E-\epsilon_o)}\begin{Bmatrix}E\\ t(\mathbf{k})\end{Bmatrix}.$$

The poles in the above expression should be avoided in the usual way by replacing $E \to E + i\eta$.

Considering only low-energy physics of the Hamiltonian, we expand momentum vector $\mathbf{k}$ near the two Dirac points, $\mathbf{k} = \mathbf{K}_\pm + \mathbf{q}$. Summation over momentum vectors then gives

$$E = \frac{\epsilon_o \pm \alpha_0 v|\sin(\theta_{AB})|/R}{\alpha_0\left(\ln|t/\epsilon_o| + i\frac{\pi}{2}\right)+1}, \qquad \alpha_0 = \frac{\gamma^2 A_o}{\pi v^2}. \quad (7)$$

Here $\theta_{AB}(\boldsymbol{R}) = \phi + \frac{2\pi R}{3\sqrt{3}a}\cos\phi$, where ϕ is the angle measured from zigzag direction as shown in Fig. 1. The dimensionless constant $\alpha_0 \sim \gamma^2/t^2$ describes the strength of hybridization relative to the hopping integral. Importantly, one

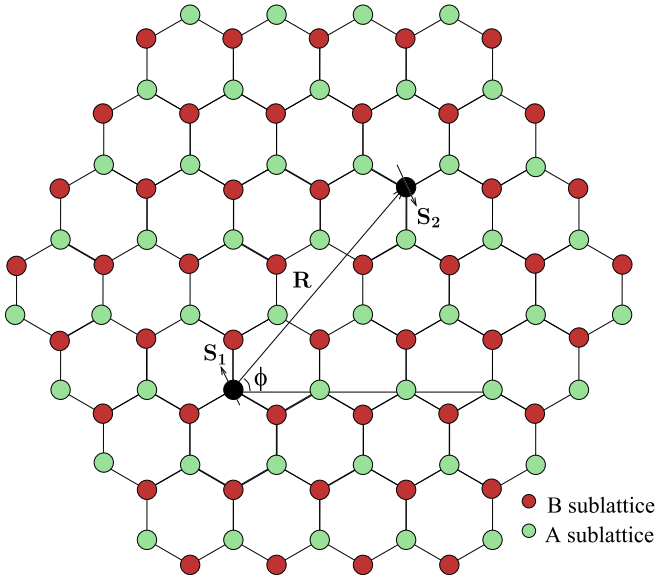

FIG. 1. Graphene honeycomb structure consisting of two sublattices A (green) and B (red). Two impurities sitting on top of the carbon atoms with spin S_1 and S_2 are shown in black and are separated by vector $\mathbf{R}$. ϕ is the angle made by the $\mathbf{R}$ with zigzag direction.

of the impurity levels in AB configuration can cross the Dirac point at a particular distance $R \sim \alpha_0 v/\epsilon_o$. As we will see in Sec. IV, the spin-exchange coupling between impurities residing on different sublattices can become resonantly enhanced at this distance where crossing occurs.

III. INTERACTION ENERGY: POTENTIAL PART

The interaction energy of conduction electrons described by the Anderson Hamiltonian Eq. (1) can be calculated using the following well-known quantum-mechanical identity:

$$\frac{\partial W}{\partial \gamma} = \left\langle \frac{\partial H}{\partial \gamma} \right\rangle = \sum_{j=1,2} \langle \hat{d}^\dagger(\mathbf{r}_j)\hat{\psi}(\mathbf{r}_j) + \hat{\psi}^\dagger(\mathbf{r}_j)\hat{d}(\mathbf{r}_j)\rangle. \quad (8)$$

This identity can be written in terms of electron Green's function:

$$\mathcal{G}(\mathbf{r}, \mathbf{r}', t) = -i\langle T\hat{\psi}(\mathbf{r}, t)\hat{\psi}^\dagger(\mathbf{r}', 0)\rangle. \quad (9)$$

Because, according to Eqs. (4) and (5), $\hat{d}(\mathbf{r}_j) = \gamma\hat{\psi}(\mathbf{r}_j)/(E - \epsilon_0)$, we obtain from Eq. (8):

$$\frac{\partial W}{\partial \gamma} = -\frac{2i\gamma}{E - \epsilon_o} \sum_{j=1,2} \mathcal{G}(\mathbf{r}_j, \mathbf{r}_j, t = 0^-). \quad (10)$$

The equation for Green's function in the energy representation is

$$E\mathcal{G}_E(\mathbf{r}, \mathbf{r}') - t\sum_i \mathcal{G}_E(\mathbf{r} + \boldsymbol{a}_i, \mathbf{r}') - \gamma(E)\delta_{\mathbf{r},0}\mathcal{G}_E(0, \mathbf{r}') - \gamma(E)\delta_{\mathbf{r},\mathbf{R}}\mathcal{G}_E(\mathbf{R}, \mathbf{r}') = \delta_{\mathbf{r},\mathbf{r}'}, \quad (11)$$

where we introduced the shorthand:

$$\gamma(E) = \frac{\gamma^2}{E - \epsilon_o}. \quad (12)$$

The solution of Eq. (11) has been found elsewhere [36] for the case of two impurities with the onsite potential U. Because the present case differs from that situation only by the replacement $U \to \gamma(E)$, we can use the result of Ref. [36],

$$\mathcal{G}_E(\mathbf{R}, 0) = G_E(\mathbf{R}, 0)\frac{1 + 2T_E G_E(0, 0) + T_E^2 G_E^2(0, 0)}{1 - T_E^2 G_E^2(0, \mathbf{R})G_E(\mathbf{R}, 0)}, \quad (13)$$

which expresses the two impurity Green's function $\mathcal{G}_E$ (for the electron propagation between two impurities) via the free-electron Green's function G_E.

The interaction energy (that part of W that depends on the distance $\mathbf{R}$ between impurities) then follows from Eq. (10):

$$W(\mathbf{R}) = 2i\int_{-\infty}^{\infty} \frac{dE}{2\pi} \ln\left[1 - T_E^2 G_E(\mathbf{R}, 0)G_E(0, \mathbf{R})\right], \quad (14)$$

where T_E stands for the T matrix:

$$T_E = \frac{\gamma(E)}{1 - \gamma(E)G_E(0, 0)}. \quad (15)$$

The free-electron Green's function evaluated at coinciding points $\mathbf{r} = \mathbf{r}' = 0$ is

$$G_E(0, 0) = -\frac{EA_0}{\pi v^2}\left[\ln\left(\frac{t}{|E|}\right) + i\frac{\pi}{2}\operatorname{sgn} E\right]. \quad (16)$$

Using now the fact that the time-ordered Green's functions do not have singularities in the first and third quadrants of the complex E plane, and rotating the integration path counterclockwise by the angle $\pi/2$ so it follows the imaginary axis, $E = i\omega$, we obtain the expression for the interaction energy,

$$W(\mathbf{R}) = -2\int_{-\infty}^{\infty} \frac{d\omega}{2\pi} \ln\left[1 - T_{i\omega}^2 \Pi_{i\omega}(\mathbf{R})\right], \quad (17)$$

where we introduced the following shorthand for the product of two Green's functions:

$$\Pi_{i\omega}(\mathbf{R}) = G_{i\omega}(0, \mathbf{R})G_{i\omega}(\mathbf{R}, 0). \quad (18)$$

For the AA configuration of adatoms [35,36],

$$\Pi_{i\omega}(\mathbf{R}) = -\frac{\omega^2 A_o^2}{\pi^2 v^4} K_0^2\left(\frac{|\omega|R}{v}\right)\cos^2\theta_{AA}, \quad (19)$$

where K_0 is the Macdonald function of the zeroth order and $\theta_{AA}(\boldsymbol{R}) = \frac{2\pi R}{3\sqrt{3}a}\cos\phi$. For AB configuration, the product is given by [35,36]

$$\Pi_{i\omega}(\mathbf{R}) = \frac{\omega^2 A_o^2}{\pi^2 v^4} K_1^2\left(\frac{|\omega|R}{v}\right)\sin^2\theta_{AB}, \quad (20)$$

where K_1 is the Macdonald function of the first order and θ_{AB} is defined after Eqs. (7).To make subsequent calculations of the energy $W(R)$ given by Eq. (17) more compact, let us introduce the two dimensionless parameters,

$$\alpha = \frac{\alpha_0}{1 + \alpha_0 \ln\left(\frac{R}{a}\right)}, \qquad \beta = \frac{R}{v}\frac{\epsilon_o}{1 + \alpha_0 \ln\left(\frac{R}{a}\right)}, \quad (21)$$

namely, the renormalized impurity coupling strength α and the parameter β that characterizes the location of the impurity level ϵ_o relative to the energy scale v/R of the electron travel between the impurities. With increasing the "bare" coupling

α_0, the renormalized α approaches a (distance-dependent) constant. Note that in the long-range limit $R \gg a$, to which the present theory only applies, α is always less than 1. The parameter β, as we are about to see, describes the effective strength of the impurity with large $\beta > 1$ corresponding to the weak impurity limit and $\beta < 1$ to the strong coupling domain.

The potential interaction energy expression for impurities residing on different sublattices in terms of α and β is given by

$$W_{AB}(\mathbf{R}) = -\frac{2v}{R}\int_{-\infty}^{\infty}\frac{dx}{2\pi}\ln\left(1-\frac{\alpha^2x^2K_1^2(|x|)\sin^2\theta_{AB}}{(ix-\beta)^2}\right). \tag{22}$$

In deriving the above expression, we have used Eq. (20) for the product of two Green's functions and the expression for the T matrix given by Eqs. (15) and (12). The integral in Eq. (22) can be calculated in different limits of α and β.

(i) When the distance between the impurities is large enough so $\beta \gg 1$, we can neglect x in the denominator and calculate the remaining integral by expanding the logarithms over a small ratio α/β (as explained before, $\alpha < 1$):

$$W_{AB}(\mathbf{R}) \approx \frac{-2v}{R}\int_{-\infty}^{\infty}\frac{dx}{2\pi}\ln\left[1-\left(\frac{\alpha}{\beta}\right)^2x^2K_1^2(|x|)\sin^2\theta_{AB}\right]$$
$$\approx \frac{3\pi\alpha_0^2}{16}\frac{v^3}{R^3\epsilon_o^2}\sin^2\theta_{AB}. \tag{23}$$

This is simply the weak impurity limit, where interaction decays with the distance as $1/R^3$, just like in a case of a substitution impurity. The interaction is positive (repulsive) there. This regime is also realized when the impurity level ϵ_o is sufficiently far away from the Dirac point.

(ii) As the distance R decreases or, alternatively, the energy level ϵ_o approaches the Dirac point, a situation of small $\beta \ll 1$ is eventually realized. (This condition means that the impurity level has the energy, $\epsilon_o \ll v/R$, i.e., much smaller than the energy corresponding to the distance R). In the most interesting case of $\alpha \ll 1$, two scenarios can occur, depending on how β compares with α. In the limit of $\alpha \ll \beta \ll 1$, one can still expand the logarithm in the integrand,

$$W_{AB}(\mathbf{R}) \approx \frac{v\alpha^2\sin^2\theta_{AB}}{\pi R}\int_{-\infty}^{\infty}dx\frac{x^2K_1^2(|x|)}{(ix-\beta)^2}, \tag{24}$$

even though it is no longer possible to neglect ix in comparison to β in the denominator. Because this limit requires small γ, the difference between two coupling constants becomes insignificant, $\alpha \approx \alpha_0$, whereas $\beta \approx \epsilon_o R/v$. The remaining integral is calculated in Appendix A to give

$$W_{AB}(\mathbf{R}) = \frac{\pi\alpha_0^2 v}{2R}\sin^2\theta_{AB}\left[1+\frac{4\epsilon_o R}{\pi v}\ln\left(0.89\frac{\epsilon_o R}{v}\right)\right]. \tag{25}$$

The sign of the interaction remains the same as in Eq. (23) but the dependence on R changes from $1/R^3$ to a long-range $1/R$. As should be, the two expressions, Eqs. (23) and (25), become of the same order when $\beta \sim 1$; this happens when $\epsilon_o \sim v/R$. Note that this situation of the *repulsive* interaction W_{AB} described by Eq. (25) does not occur in case of potential substitutional impurities where W_{AB} always remains attractive.

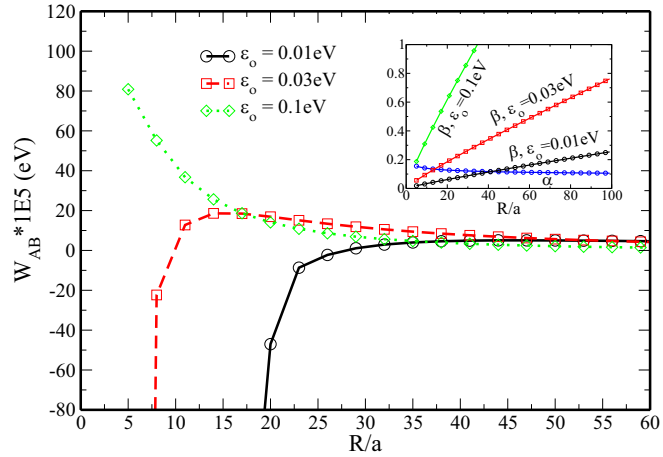

FIG. 2. Interaction energy is plotted as a function of distance between the impurities R/a in AB configuration for three different values of on-site energy ϵ_o: 0.01, 0.03, and 0.1 eV. The coupling constant $\gamma = 1$ eV is same for all three plots in this figure. It is exact numerical plot of Eq. (22).

In the second limit of $\beta \ll \alpha \ll 1$, where the impurity-level energy ϵ_o is negligible in comparison with v/R, it is appropriate to ignore β in the integrand in Eq. (22):

$$W_{AB}(\mathbf{R}) \approx -\frac{2v}{R}\int_0^{\infty}\frac{dx}{\pi}\ln\left[1+\alpha^2\sin^2\theta_{AB}K_1^2(x)\right]$$
$$\approx -\frac{2v}{R}\int_0^{\infty}\frac{dx}{\pi}\ln\left(1+\frac{\alpha^2\sin^2\theta_{AB}}{x^2}\right). \tag{26}$$

Since the relevant values of x in this integral are of the order of α, neglecting β in the original integral is justified. Utilizing also that α is small, we used the small-argument expansion of the Macdonald function, $K_1(x) \sim 1/x$. The remaining integral is straightforward to calculate using integration by parts and is equal to $\pi\alpha|\sin(\theta_{AB})|$. The expression of interaction energy is thus given by

$$W_{AB}(\mathbf{R}) = -\frac{2\alpha v}{R}|\sin\theta_{AB}|. \tag{27}$$

Note that the presence of the logarithmic term in α indicates the onset of multiple scattering of electrons off the impurities. This is the strong impurity limit where the interaction is attractive, in contrast to the weak impurity limit. In the limit of $\alpha_0\ln(R/a) \gg 1$, we recover the expression found earlier in Refs. [35,36] for strong potential impurities.

Figure 2 illustrates the dependence of W_{AB} on the distance between impurities for different values of on-site energy ϵ_o: 0.1, 0.03, and 0.01 eV and coupling $\gamma = 1$ eV. The inset plot in the figure is to explain the behavior of interaction energy with the help of impurity strength parameter β and renormalized impurity coupling α. It shows the variation of β with distance R/a for the above set of on-site energies ϵ_o along with α plotted for $\gamma = 1$ eV. For $\epsilon_o = 0.1$ eV, β remains greater than α for all values of R/a, hence the interaction energy is always repulsive. As we decrease ϵ_o to 0.03 eV and further down to 0.01 eV, we see the transition from weak coupling to strong coupling occurs, leading to attractive interaction. It happens

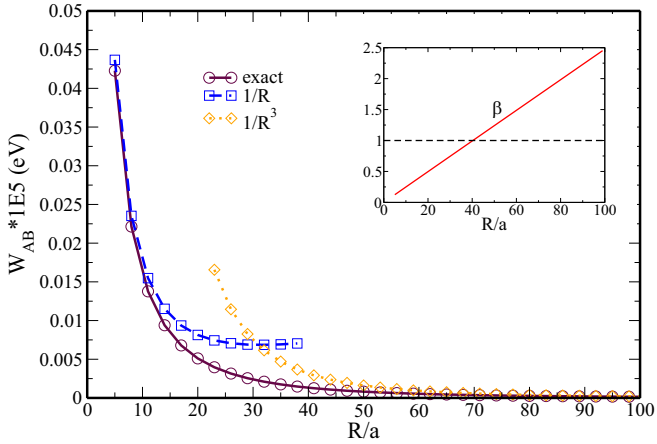

FIG. 3. Interaction energy is plotted as a function of distance between the impurities R/a in AB configuration for on-site energy $\epsilon_o = 0.05$ eV and coupling constant $\gamma = 0.1$ eV. The first plot labeled *exact* is a result of the exact numerical integration Eq. (22). The other two plots labeled $1/R$ and $1/R^3$ are plotted using Eqs. (25) and (23), respectively.

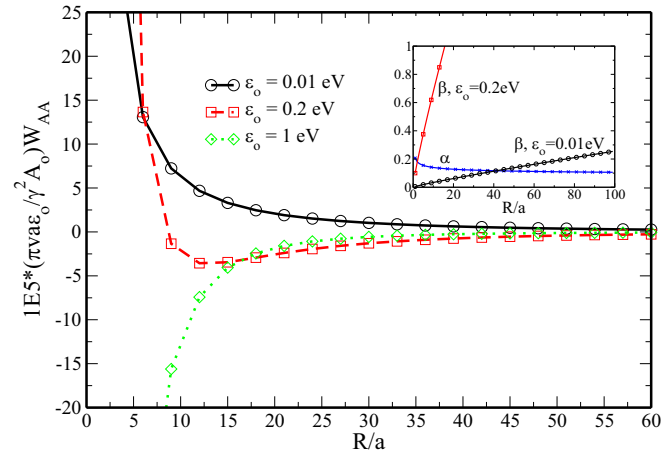

FIG. 4. Interaction energy W_{AA} is plotted as a function of distance between the impurities R/a in AA configuration for three different values of on-site energy ϵ_o: 0.01, 0.2, and 1 eV. The coupling constant $\gamma = 1$ eV is same for all three plots in this figure. W_{AA} is scaled by dimensionless ratio $\pi v a \epsilon_o/\gamma^2 A_o$. It is the exact numerical plot of Eq. (28).

at the value of R/a when $\beta \sim \alpha$. Figure 3, on the other hand, shows the dependence of W_{AB} on the distance in different regimes. Even though the potential interaction in this regime is repulsive, it changes from $1/R$ to $1/R^3$ dependence at $\beta \sim 1$.

The interaction energy for the two impurities residing on same sublattices is given by

$$W_{AA}(\mathbf{R}) = \frac{-2v}{R}\int_{-\infty}^{\infty}\frac{dx}{2\pi}\ln\left(1+\frac{\alpha^2 x^2 K_0^2(|x|)\cos^2\theta_{AA}}{(ix-\beta)^2}\right). \tag{28}$$

As in the AB case, we calculate the above integral in different limits of α and β. In the weak impurity limit, $\beta \gg 1$, the integrand is simplified by neglecting x in the denominator and the remaining integral can be calculated by expansion of the log:

$$\begin{aligned} W_{AA}(\mathbf{R}) &\approx \frac{-2v}{R}\int_{-\infty}^{\infty}\frac{dx}{2\pi}\ln\left[1+\left(\frac{\alpha}{\beta}\right)^2 x^2 K_0^2(|x|)\right] \\ &\approx -\frac{\pi\alpha_o^2}{16}\frac{v^3}{R^3\epsilon_o^2}\cos^2\theta_{AA}. \end{aligned} \tag{29}$$

Because the integral converges over $x \sim 1 \ll \beta$, neglecting x in comparison to β in the denominator is justified. The interaction in the AA configuration in the weak impurity limit is attractive, in contrast to the repulsive interaction in the AB case, and is three times smaller in magnitude.

When $\beta \ll 1$, similar to the AB case, two limits arise: (i) For $\alpha \ll \beta \ll 1$, we are still justified to expand the logarithm (but not to neglect x in the denominator):

$$W_{AA}(\mathbf{R}) \approx \frac{v\alpha^2\cos^2\theta_{AA}}{\pi R}\int_{-\infty}^{\infty} dx \frac{x^2 K_0^2(|x|)}{(x+i\beta)^2}. \tag{30}$$

The above integral is calculated in Appendix A and the expression of interaction energy is given by

$$\begin{aligned} W_{AA}(\mathbf{R}) = \frac{v\alpha^2\cos^2\theta_{AA}}{\pi R}\Bigg[&\frac{\pi}{2} - \frac{\pi^2}{2}\frac{\epsilon_o R}{v} \\ &- \frac{2\epsilon_o R}{v}\ln^2\left(\frac{\epsilon_o R}{v}\right) - \frac{2\epsilon_o R}{v}\ln\left(\frac{\epsilon_o R}{v}\right)\Bigg]. \end{aligned} \tag{31}$$

(ii) In the remaining limit of $\beta \ll \alpha \ll 1$, we can neglect β in denominator of the integral in Eq. (30) and obtain

$$W_{AA}(\mathbf{R}) = \frac{\pi\alpha^2 v}{2R}\cos^2\theta_{AA}. \tag{32}$$

We see that in the strong impurity limit the interaction is repulsive, in contrast to the weak impurity limit Eq. (29) where it is attractive.

Figure 4 illustrates the dependence of W_{AA} on the distance between impurities for different values of the on-site energy ϵ_o: 1, 0.2, 0.01 eV and coupling $\gamma = 1$ eV. The inset plot in the figure is to explain the behavior of interaction energy with the help of impurity strength parameter β and renormalized impurity coupling α. It shows the variation of β with distance R/a for the above set of on-site energies ϵ_o along with α plotted for $\gamma = 1$ eV. For $\epsilon_o = 1$ eV, β remains greater than one for all values of R/a, hence the interaction energy is always attractive. As we decrease ϵ_o to 0.2 eV and further down to 0.01 eV, we see the transition from weak coupling to strong coupling occurs leading to repulsive interaction. It happens at the value of R/a when $\beta \sim \alpha$. Figure 5, on the other hand, shows the dependence of W_{AA} on the distance in a different regime. The potential interaction in this regime changes from attractive, $1/R^3$, to repulsive, $1/R$, at $\beta \sim 1$.

IV. INTERACTION ENERGY: SPIN-DEPENDENT PART

To describe a spin-dependent part of the interaction between Anderson magnetic impurities in graphene, we add to

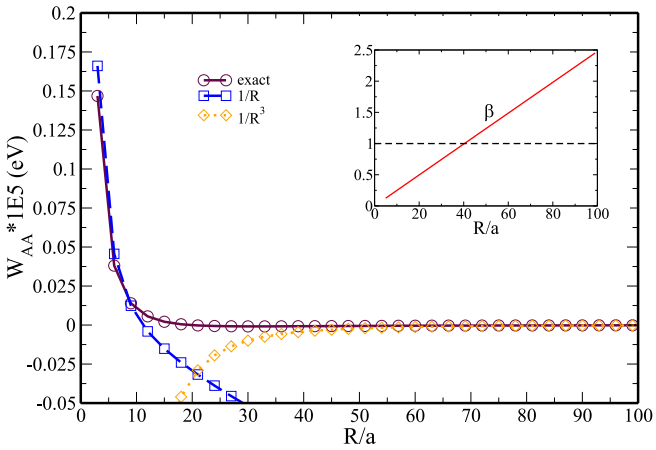

FIG. 5. Interaction energy is plotted as a function of distance between the impurities R/a in AA configuration for on-site energy $\epsilon_o = 0.05$ eV and coupling constant $\gamma = 0.1$ eV. The first plot labeled *exact* is a result of the exact numerical integration Eq. (28). The other two plots labeled $1/R$ and $1/R^3$ are plotted using Eqs. (31) and (29), respectively.

our Hamiltonian the spin term

$$H = H_a + H_{\rm sp}, \tag{33}$$

where H_a is given by Eq. (1) and

$$H_{\rm sp} = J\mathbf{S_1}\cdot\hat\psi^\dagger_\alpha(0)\hat{\boldsymbol\sigma}_{\alpha\beta}\hat\psi_\beta(0) + J\mathbf{S_2}\cdot\hat\psi^\dagger_\alpha(\mathbf{R})\hat{\boldsymbol\sigma}_{\alpha\beta}\hat\psi_\beta(\mathbf{R}) \tag{34}$$

contains two short-range exchange interactions between spins of impurities, $\mathbf{S}_1$, $\mathbf{S}_2$, and those of conduction electrons described by the Pauli matrices $\hat{\boldsymbol\sigma}$. The exchange coupling J is assumed to be small compared with both t and γ. As a result of the coupling to conduction electrons, there appears the effective coupling of impurity spins,

$$H_{\rm eff} = J_{\rm eff}(\mathbf{R})\,\mathbf{S}_1\cdot\mathbf{S}_2. \tag{35}$$

The effective exchange constant $J_{\rm eff}$ can be obtained from the already familiar method of differentiation with respect to the coupling parameter J,

$$\frac{\partial J_{\rm eff}}{\partial J}\mathbf{S}_1\cdot\mathbf{S}_2 = \left\langle\frac{\partial H}{\partial J}\right\rangle = \sum_{j=1,2}\mathbf{S}_j\cdot\langle\hat\psi^\dagger(\mathbf{r}_j)\hat{\boldsymbol\sigma}\hat\psi(\mathbf{r}_j)\rangle. \tag{36}$$

The expectation values in Eq. (36) should be calculated to the lowest (first) order in the Hamiltonian Eq. (34). This yields

$$J_{\rm eff} = -2iJ^2\int_{-\infty}^{\infty}\frac{dE}{2\pi}\mathcal{G}_E(\mathbf{R},0)\mathcal{G}_E(0,\mathbf{R}). \tag{37}$$

The last expression can be simplified further by expressing Green's functions via free-electron Green's functions, Eq. (13). At last, rotating the integration path counterclockwise by the angle $\pi/2$, $E = i\omega$, we obtain

$$J_{\rm eff} = \frac{J^2}{\pi}\int_{-\infty}^{\infty}d\omega \times\frac{\Pi_{i\omega}(\mathbf{R})}{[(1-\gamma(i\omega)G_{i\omega}(0,0))^2-\gamma^2(i\omega)\Pi_{i\omega}(\mathbf{R})]^2}. \tag{38}$$

Having obtained the general expression for the effective spin-exchange coupling for two impurities in the AA or AB configuration, we can now proceed with evaluating it for different limits of the coupling strength γ and the position of the impurity level ϵ_o.

A. *AB* configuration

We begin by calculating spin-exchange coupling in AB configuration using Eq. (20) for the product of two Green's functions $\Pi(\mathbf{R})$ and $\gamma(i\omega) = \gamma^2/(i\omega-\epsilon_o)$. The Green's function at coinciding points $G_{i\omega}(0,0)$ is given by Eq. (16). To simplify calculations further, let us introduce dimensionless distance $\rho = \epsilon_o R/v\alpha_0$ as [here, $\alpha_o = \gamma^2 A_o/\pi v^2$, defined earlier in Eqs. (7)]:

$$J^{AB}_{\rm eff}(\mathbf{R}) = \frac{J^2}{\pi^3\alpha_0^4}\frac{A_o^2}{vR^3}\sin^2\theta_{AB}\int_{-\infty}^{\infty}\frac{dx x^2K_1^2(|x|)(ix-\alpha_0\rho)^4}{\left[\left(\rho - ix\left(\frac{1}{\alpha_0}+\ln\left[\frac{R}{a|x|}\right]\right)\right)^2-\sin^2\theta_{AB}x^2K_1^2(|x|)\right]^2}. \tag{39}$$

Below we consider the dependence of the effective exchange constant on the distance R (represented by the dimensionless variable ρ), as predicted by Eq. (39).

At both large and small distances R, we obtain the same power-law dependence, $J_{AB}\propto 1/R^3$. Indeed, for very large ρ, the integral in Eq. (39) is equal to $\alpha_0^4\int_{-\infty}^{\infty}dx x^2K_1^2(|x|) = 3\pi^2\alpha_0^4/16$, so the exchange coupling becomes

$$J^{AB}_{\rm eff}(\mathbf{R}) = \frac{3J^2}{16\pi}\frac{A_o^2}{vR^3}\sin^2\theta_{AB}. \tag{40}$$

The applicability of this expression follows from the observation that $x\sim 1$ contributes to the integral and that ρ must be large enough compared with $\frac{1}{\alpha_0}+\ln\frac{R}{a}$, or in terms of the actual distance, $R\gg(v/\epsilon_o)(1+\alpha_0\ln\frac{R}{a})$.

On the other hand, at small distances one can simply set $\rho\to 0$ in the integral. This again reveals the R^{-3} dependence as the integral still converges at $x\sim 1$. Provided that $\frac{1}{\alpha_0}+\ln\frac{R}{a}\gg 1$, one can also neglect the $K_1^2(|x|)\sim 1$ term in the denominator. The exchange constant then assumes the form

$$J^{AB}_{\rm eff}(\mathbf{R}) = \frac{3J^2}{16\pi}\frac{A_o^2}{vR^3}\frac{\sin^2\theta_{AB}}{\left(1+\alpha_0\ln\frac{R}{a}\right)^4}. \tag{41}$$

The short-distance value Eq. (41) is suppressed, compared with the long-distance asymptotic Eq. (40), by the additional factor that depends weakly (logarithmically) on R. To justify neglecting ρ in both the numerator and the denominator, it is sufficient to have $\alpha_0\rho\ll 1$ or, equivalently, $R\ll v/\epsilon_o$. The $1/R^3$ increase of the exchange constant at short distances described by Eq. (41) does not occur in the case of substitutional impurities [37]. In the latter case, where at small distance

a strong impurity limit is realized, is characterized by the exchange constant decreasing with decreasing distance R.

At $\rho \to 0$, the contribution of $x \sim 1$ to the integral in Eq. (39) is the only one that matters, and leads to Eq. (41). However, as ρ increases (but still does not exceed 1, see below), a contribution of small $x \ll 1$ might become dominant, where the term ix in the numerator of the integrand can be neglected in comparison with $\alpha_0\rho$ and where one can approximate $K_1(x) \approx 1/x$. As long as the poles of the integrand are on opposite sides of the real axis (see discussion below), the remaining integral can be calculated by the residue method:

$$J_{\text{eff}}^{AB}(\mathbf{R}) = \frac{J^2}{\pi^3}\frac{A_o^2}{\upsilon R^3}\left(\frac{\epsilon_o R}{\upsilon\alpha_0}\right)^4 \sin^2\theta_{AB} \times \int_{-\infty}^{\infty} \frac{dx}{\left[\left(\rho - ix\ln\left[\frac{cR}{a|x|}\right]\right)^2 - \sin^2\theta_{AB}\right]^2} = \frac{\pi^2 J^2}{2\pi^2}\frac{\epsilon_o^4 \upsilon^3 R}{A_o^2\gamma^8}\frac{1}{|\sin\theta_{AB}|\ln\left(\frac{\alpha_0\upsilon}{a\epsilon_o}\right)}. \quad (42)$$

Because $\sin\theta_{AB} \sim 1$, the typical value $x \sim 1/\ln(R/a)$ and the condition $x \ll 1$ is satisfied automatically. But to ensure that x is smaller than $\alpha_0\rho$, one must also have $\alpha_0\rho \gg 1/\ln\frac{R}{a}$ or, equivalently, $R \gg (\upsilon/\epsilon_o)/\ln\frac{R}{a}$. We conclude that the exchange coupling constant is the sum of contributions Eqs. (41) and (42) in the range of distances, $(\upsilon/\epsilon_o)/\ln\frac{R}{a} \ll R \ll \upsilon/\epsilon_o$. Within this range, with increasing R, the $\propto R^{-3}$ contribution gradually becomes dominated by the linear $\propto R$ term. The crossover occurs at the point where the two terms are of the same order of magnitude, at $R \sim (\upsilon/\epsilon_o)/(\ln\frac{R}{a})^{3/4}$.

One additional condition should be emphasized. The residue method applies only if $\rho < \rho_0 = |\sin\theta_{AB}|$ or equivalently $R < \gamma^2 A_0|\sin\theta_{AB}|/\pi\upsilon\epsilon_o$; otherwise, the poles of the integrand in Eq. (42) reside on the same side of the real axis. To ensure that one nonetheless has $\alpha_0\rho\ln\frac{R}{a} \gg 1$, it is necessary that the value $\alpha_0 \sim (\gamma/t)^2$ is not too small, i.e., that $\alpha_0\ln\frac{R}{a} \gg 1$.

The linear increase of the effective spin-exchange coupling is caused by multiple scattering of conduction electrons off the two impurities. As the distance ρ increases even further and approaches $\rho_0 = |\sin\theta_{AB}|$, a resonant enhancement of the exchange constant occurs. There, one of the energy levels of the impurities in AB configuration crosses the Dirac point, see Eqs. (7). As a result, at $\rho = \rho_0$ the integrand has the singularity at $x = 0$. For small values $\rho - \rho_o$, the integral can be calculated by keeping only terms linear in x in the denominator. This is justified by the fact that the integral converges at $x \sim (\rho^2 - \rho_0^2)/(\rho_0\ln\frac{R}{a})$. In the leading logarithm approximation we obtain (see Appendix B for details)

$$J_{\text{eff}}^{AB}(\mathbf{R}) = -\frac{\upsilon J^2\epsilon_o^2}{4\gamma^4|R - R_0|}\frac{|\sin\theta_{AB}|}{\ln^2\left(\frac{R_0^2}{a(R-R_0)}\right)}. \quad (43)$$

Figure 6 illustrates the dependence of the spin-exchange coupling J_{AB} on the distance between the impurities for different values of the on-site energy ϵ_o and $\gamma = 3$ eV. The interaction changes from the weak impurity limit to strong impurity limit at short distances on decreasing value of ϵ_o. This can be understood from the inset plot shown inside the graph,

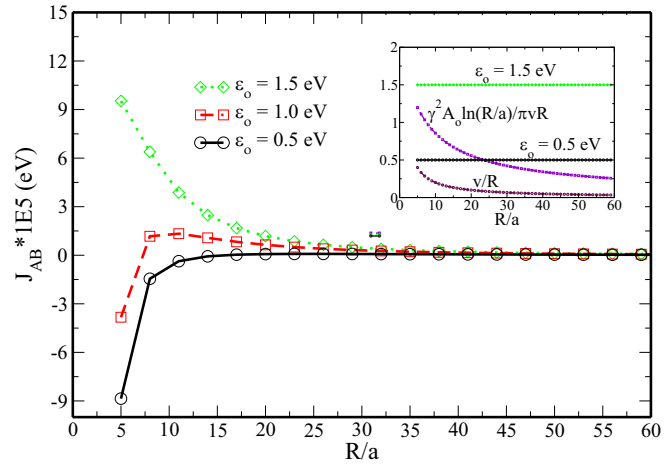

FIG. 6. Effective spin coupling is plotted as a function of distance between the impurities R/a in AB configuration for three different values of on-site energy ϵ_o: 0.5, 1.0, and 1.5 eV. The coupling constant $\gamma = 3$ eV is the same for all three plots in this figure. It is the exact numerical plot of Eq. (39).

it shows the variation of $\gamma^2 A_o\ln(R/a)/\pi\upsilon R$ and υ/R with R/a. ϵ_o is always greater than $\gamma^2 A_o\ln(R/a)/\pi\upsilon R$ for $\epsilon_o = 1.5$ eV and thus the interaction is always antiferromagnetic. It changes to strong impurity limit for $R \sim \gamma^2 A_o\ln(R/a)/\pi\upsilon\epsilon_o$ for $\epsilon_o = 0.5$ eV where the impurities are ferromagnetically coupled.

Figure 7 illustrates the dependence of the spin-exchange coupling J_{AB} on the distance between the impurities for two values of on-site energy $\epsilon_o = 0.01$ and 0.05 eV and $\gamma = 3$ eV. At small distances $R < (\upsilon/\epsilon_o)/(\ln\frac{R}{a})^{3/4}$, the interaction is antiferromagnetic and decreases with increasing R. On increasing distance, we see a transition from weak coupling to strong coupling. Above $R \sim (\upsilon/\epsilon_o)/(\ln\frac{R}{a})^{3/4}$, the interaction remains antiferromagnetic but increases linearly with

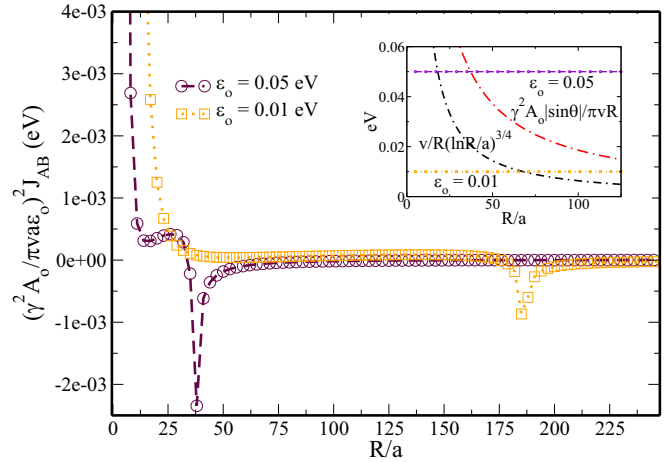

FIG. 7. Effective spin coupling J_{AB} is plotted as a function of distance between the impurities R/a in AB configuration for two different values of on-site energy ϵ_o: 0.01 and 0.05 eV. The coupling constant $\gamma = 3$ eV is same for all three plots in this figure. J_{AB} is scaled by dimensionless ratio $\gamma^2 A_o/\pi\upsilon a\epsilon_o$. It is the exact numerical plot of Eq. (39).

R. At $R = \gamma^2 A_0 |\sin\theta_{AB}|/\pi v\epsilon_o$, the spin-exchange coupling becomes resonant ferromagnetic.

B. *AA* configuration

In the *AA* configuration of impurities, the spin exchange coupling is given by

$$J^{AA}_{\rm eff}(\mathbf{R}) = -\frac{J^2}{\pi^3\alpha_0^4}\frac{A_o^2}{vR^3}\cos^2\theta_{AA}\int_{-\infty}^{\infty} dx \frac{x^2K_0^2(|x|)(ix-\alpha_0\rho)^4}{\left[\left(\rho + ix\left(\frac{1}{\alpha_0}+\ln\left[\frac{R}{a|x|}\right]\right)\right)^2 + \cos^2\theta_{AA}x^2K_0^2(|x|)\right]^2}. \tag{44}$$

Similar to the *AB* case, we obtain the same $1/R^3$ dependence of spin-exchange coupling for both small and large distances R. For large $\rho \gg \frac{1}{\alpha_0}+\ln(\frac{R}{a})$, we can keep only the ρ terms in both numerator and denominator and utilize the fact that the integral in Eq. (44) converges at $x \sim 1$. Because $\int_{-\infty}^{\infty} dx x^2K_0^2(|x|) = \pi^2/16$, the exchange coupling becomes

$$J^{AA}_{\rm eff}(\mathbf{R}) = -\frac{J^2}{16\pi}\frac{A_o^2}{vR^3}\cos^2\theta_{AA}. \tag{45}$$

On the other hand, for small $\rho \to 0$ and large value of $\frac{1}{\alpha_0}+\ln(\frac{R}{a}) \gg 1$, we can neglect in the denominator both ρ and the term containing $K_0(x)$:

$$J^{AA}_{\rm eff}(\mathbf{R}) = -\frac{J^2}{16\pi}\frac{A_o^2}{vR^3}\frac{\cos^2\theta_{AA}}{\left(1+\alpha_0\ln\frac{R}{a}\right)^4}. \tag{46}$$

Again $x \sim 1$ values determine the integral, and thus the last expression is valid as long as $\alpha_0\rho \ll 1$, which is equivalent to $R \ll v/\epsilon_o$. Unlike in the case of substitutional impurities [37], the small-distance $1/R^3$ dependence of the exchange coupling constant is similar to the large-distance perturbative expression, but is suppressed by the factor $(1+\alpha_0\ln R/a)^4$.

As ρ increases, the contribution of small $x \ll 1$ can become important, where we can neglect ix term in the numerator in comparison to $\alpha_0\rho$. For $\rho \ll 1$, the integral in Eq. (44) converges on $x \sim \rho$ where we can approximate the Macdonald function $K_0(x) \approx -\ln x$. In the leading logarithmic approximation, it is typically sufficient to take the logarithms at the characteristic arguments; in this case, $x \sim \rho$. But the integral thus evaluated will vanish because both poles of the integrand will lie on the same side of the x axis. Thus, it is important to calculate the subleading contribution to the integral where one can no longer treat logarithms as constant. The corresponding calculation is presented in Appendix C. In the limit of small ϵ_o and large distances R, it amounts to

$$J^{AA}_{\rm eff}(\mathbf{R}) = \frac{2J^2\pi v^2\epsilon_o^3}{3A_0\gamma^6}\ln\left(\frac{v\alpha_0}{R\epsilon_o}\right)\frac{\cos^2\theta_{AA}}{\ln^3\left(\frac{v\alpha_0}{a\epsilon_o}\right)}. \tag{47}$$

We note that since $x \sim \rho$, the condition $\alpha_0\rho \gg x$ requires that the value of α_0 is large, $\alpha_0 \gg 1$. If this is the case, the exchange coupling constant for $R \ll v/\epsilon_o$ is the sum of two contributions, Eqs. (46) and (47). With increasing R, the logarithmic contribution Eq. (47) exceeds the R^{-3} part, Eq. (46). This crossover occurs when the two terms becomes of the same order, at $R \sim \frac{v}{\epsilon_o}\ln(\frac{v\alpha_o}{a\epsilon_o})[\frac{t}{\gamma(\ln R/a)^2}]^{2/3}$.

Figure 8 illustrates dependence of the spin-exchange coupling J_{AA} on the distance between impurities for $\gamma = 3$ eV and different values of the on-site energy ϵ_o. The impurities are ferromagnetically coupled for large distances R. The change from weak to strong impurity occurs at distances $R \sim \gamma^2 A_o \ln(R/a)/\pi v\epsilon_o$ as seen from the inset plot. The impurities are antiferromagnetically coupled in the strong impurity limit until $\epsilon_o \ll v/R$, where it switches back to ferromagnetic coupling.

V. INTERACTION BETWEEN ANDERSON AND POTENTIAL IMPURITIES

Graphene can simultaneously have impurities or defects of multiple types. For example, a hydrogen atom can be present together with a lattice vacancy. In this situation, it would be important to understand how the two objects might interact, if they attract or repel each other. While the hydrogen atom is well described by a resonant Anderson impurity, the vacancy can be viewed as a potential (substitution) impurity with a very large on-site potential. What makes this case particularly interesting is the fact that the nature of the two impurities can be very different, unlike the cases considered so far, of the same-type impurities. For example, one of the impurities can be weak (small on-site potential U) while the other impurity can be resonant (for example, an Anderson impurity having the on-site energy ϵ_o close to the Dirac point).

A. Potential part of interaction

Repeating the derivation of Sec. III, we obtain that the potential energy of the interaction between a substitution

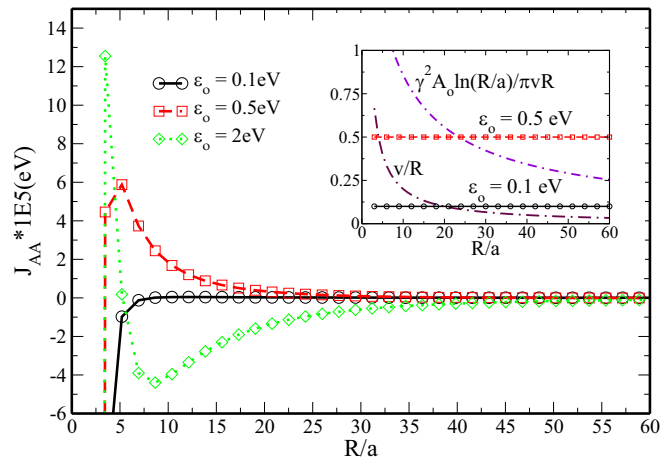

FIG. 8. Effective spin coupling J_{AA} is plotted as a function of distance between the impurities R/a in *AA* configuration for three different values of onsite energy ϵ_o: 0.1, 0.5, and 2 eV. The coupling constant $\gamma = 3$ eV is the same for all three plots in this figure. It is the exact numerical plot of Eq. (44).

impurity and an Anderson impurity is

$$W(\mathbf{R}) = -2\int_{-\infty}^{\infty}\frac{d\omega}{2\pi}\ln\left[1 - T_U(i\omega)T_\gamma(i\omega)\Pi_{i\omega}(\mathbf{R})\right], \quad (48)$$

where, T_U and T_γ are the T matrices corresponding to the scattering from the potential and the Anderson impurities, respectively: T_γ is defined in Eq. (15) and T_U is given by the same expression where γ_E is replaced with U. We consider the most interesting situation of the two impurities residing on different sublattices, where a new $1/R^2$ dependence exists when one of the impurities is a strong Anderson impurity and the other impurity is a weak potential impurity. In case of two impurities on the same sublattice, the less divergent behavior of $K_0(|x|)$, as compared to $K_1(|x|)$, for $x \ll 1$ makes it always possible to expand the logarithm, so that no new dependence on R emerges. Thus we look at the interaction energy in AB configuration,

$$W(\mathbf{R}) = -\frac{2v}{R}\int_{-\infty}^{\infty}\frac{dx}{2\pi}\ln\left(1 - \frac{\alpha u x^2 K_1^2(|x|)\sin^2\theta_{AB}}{[1 + iux\ln(\frac{R}{a|x|})](ix-\beta)}\right). \quad (49)$$

According to the definitions, Eqs. (21), the coefficient α is a number between 0 and 1, which describes how strongly the Anderson impurity is coupled to the conduction band. The distance-dependent parameter β describes the effective strength of the Anderson impurity. Finally, u is the dimensionless potential impurity strength, $u = UA_0/\pi v R$.

We first consider the case of a weak potential impurity, $u\ln(R/a) \ll 1$, where one can approximate $1 + iux\ln(\frac{R}{a|x|}) \approx 1$, as x is at most of the order 1 due to the presence of the exponentially decaying Macdonald function K_1. For a weak Anderson impurity, $\beta > 1$, the small value of u makes it possible to expand the logarithm in Eq. (49). The resulting x integral converges over $x \sim 1$ and the interaction Eq. (50) reduces to the usual perturbative form, $W \propto R^{-3}$.

If the effective strength of the Anderson impurity increases (for example, due to decreasing distance R), we enter the domain where $\beta \ll 1$. Because small values of x are important now, we can approximate $K_1(x) \sim 1/x$. The interaction energy becomes

$$W(\mathbf{R}) = -\frac{v}{R}\int_0^{\infty}\frac{dx}{\pi}\ln\frac{x^2+\beta'^2}{x^2+\beta^2}, \quad (50)$$

where $\beta' = \beta + \alpha u\sin^2\theta_{AB}$. Using the integration by parts, we obtain

$$W(\mathbf{R}) = -\frac{UA_0}{\pi R^2}\alpha\sin^2\theta_{AB}. \quad (51)$$

We see that the interaction energy in the case of a weak potential impurity and a strong Anderson impurity is proportional to $1/R^2$, in contrast to the $1/R^3$ and $1/R$ results previously seen for two identical weak and strong impurities, respectively. Interestingly, the sign of the interaction depends only on the sign of U but not on the sign of β: The actual location of the resonant level (above or below the Dirac point) is not important.

Figure 9 illustrates the dependence of W_{AB} on the distance between impurities for on-site energy $\epsilon_o = 0.005$ eV, coupling constant $\gamma = 0.1$ eV and $U = 1$ eV. For these values and range

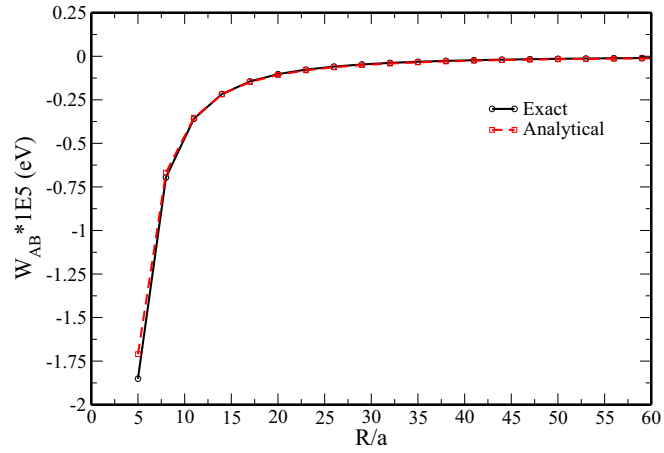

FIG. 9. Interaction energy is plotted as a function of distance between the impurities R/a in AB configuration for on-site energy $\epsilon_o = 0.005$ eV, coupling constant $\gamma = 0.1$ eV and on-site potential $U = 1$ eV. The first plot labeled *exact* is a result of the exact numerical integration Eq. (49) and the other plot labeled *analytical* is plotted using Eq. (51).

of distances shown in the plot, the potential impurity is weak while Anderson impurity is strong. The interaction energy is proportional to $1/R^2$, as given by Eq. (51) and is attractive in nature.

Next, we consider the opposite limit of a strong potential impurity, $u \gg 1$. In this limit, the T_U matrix is independent of U: $T_U \approx \frac{-i\pi v^2}{\omega A_0 \ln(t/|\omega|)}$. The interaction energy expression in this limit is given by

$$W(\mathbf{R}) = -\frac{2v}{R}\int_{-\infty}^{\infty}\frac{dx}{2\pi}\ln\left(1 + \frac{i\alpha\sin^2\theta_{AB}x^2K_1^2(|x|)}{x\ln(\frac{R}{a|x|})(ix-\beta)}\right). \quad (52)$$

In the case of a weak Anderson impurity, $\beta \gg 1$, the logarithm can be expanded and the interaction energy assumes the form $W(\mathbf{R}) \propto 1/R^3$.

When the strength of the Anderson impurity increases so that $\beta \ll 1$, the small-argument approximation of the Macdonald function can be used, $K_1(x) \sim 1/x$. Utilizing the integration by parts and changing the variable, $x = \beta y$, we reduce the remaining integral to

$$W(\mathbf{R}) = -\frac{iv\alpha\sin^2\theta_{AB}}{\pi\beta R} \times\int_{-\infty}^{\infty}dy\frac{(2iy-1)\mathcal{L}+1-iy}{(iy-1)\mathcal{L}\left[y(iy-1)\mathcal{L}+i\alpha/\beta^2\right]}, \quad (53)$$

where we denoted $\mathcal{L} = \ln(R/a\beta|y|)$. In the last integral, it is now sufficient to approximate the slowly varying logarithm with its typical value within the range of integration, $\mathcal{L} \approx \ln(R/a\beta)$; the remaining integral is elementary and yields

$$W(\mathbf{R}) = -\frac{4v\alpha\sin^2\theta_{AB}}{\beta R\mathcal{L}^2}\left(\frac{\mathcal{L}}{1+K} - \frac{1}{2K}\right), \quad (54)$$

where $K = \sqrt{1 + 4\alpha/\beta^2\mathcal{L}}$.

From the last result, we see that in the case of an Anderson impurity of intermediate strength, $\sqrt{\alpha/\mathcal{L}} \ll \beta \ll 1$, where

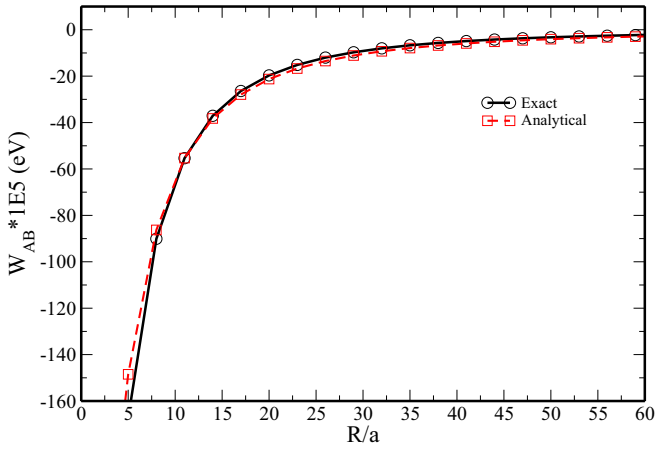

FIG. 10. Interaction energy is plotted as a function of distance between the impurities R/a in AB configuration for on-site energy $\epsilon_o = 0.005$ eV, coupling constant $\gamma = 0.1$ eV, and on-site potential $U = 50$ eV. The first plot labeled *exact* is a result of the exact numerical integration Eq. (49) and the other plot labeled *analytical* is plotted using Eq. (54).

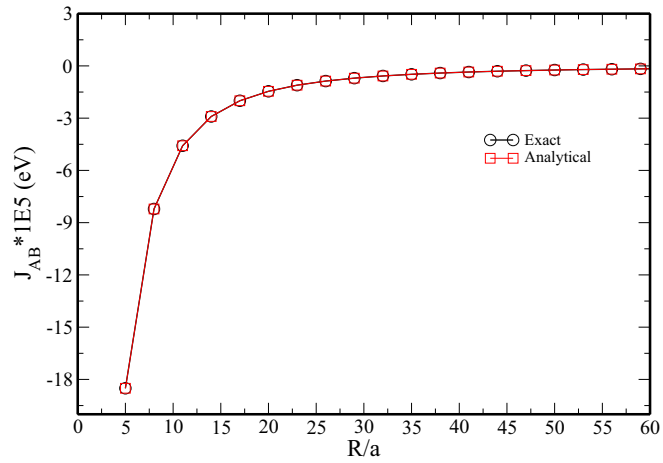

FIG. 11. Effective spin coupling J_{AB} is plotted as a function of distance between the impurities R/a in AB configuration for on-site energy $\epsilon_o = 0.5$ eV, coupling constant $\gamma = 0.1$ eV, and on-site potential $U = 100$ eV. The first plot labeled *exact* is a result of the exact numerical integration Eq. (56) and the other plot labeled *analytical* is plotted using Eq. (58).

$K \approx 1$, the interaction energy is proportional to $1/R^2$, similar to the above case of a weak potential impurity, Eq. (51), although suppressed by the factor $\ln(R/a\beta)$.

If the strength of the Anderson impurity increases even more, $\beta \ll \sqrt{\alpha/\mathcal{L}}$, so that $K \gg 1$—which happens at small distances—the dependence of the interaction energy switches to $\propto 1/R$.

Figure 10 illustrates the dependence of W_{AB} on the distance between impurities for on-site energy $\epsilon_o = 0.005$ eV, coupling constant $\gamma = 0.1$ eV, and $U = 50$ eV. For these values and the range of distances shown in the plot, the potential impurity is strong while the Anderson impurity is in the intermediately strong regime. The interaction energy is proportional to $1/R^2$, as given by Eq. (54) and is attractive in nature.

B. Spin-exchange energy

The spin interaction energy expression between a potential and an Anderson impurity can be derived by following the method of Sec. IV, which gives

$$J_{\text{eff}} = \frac{J^2}{\pi U^2}\int_{-\infty}^{\infty} d\omega \frac{\gamma^{-2}(i\omega)\,\Pi_{i\omega}(\mathbf{R})}{[T_\gamma^{-1}(i\omega)T_U^{-1}(i\omega) - \Pi_{i\omega}(\mathbf{R})]^2}. \quad (55)$$

Let us consider the more interesting case of impurities residing on different sublattices. The coupling constant is then given by

$$J_{\text{eff}}^{AB}(\mathbf{R}) = \frac{J^2 s^2 A_o^2}{\pi^3 v R^3}\int_{-\infty}^{\infty} \times \frac{dx\, x^2 K_1^2(|x|)(ifx/\alpha_0 - 1)^2}{[(1+iux\mathcal{L})(1-ixf\mathcal{L}_1) + fus^2x^2K_1^2(|x|)]^2}, \quad (56)$$

where, as before, $u = UA_0/\pi vR$ is the dimensionless strength of the potential impurity, and $\mathcal{L} = \ln\frac{R}{a|x|}$. We further introduce $\mathcal{L}_1 = 1/\alpha_0 + \mathcal{L}$. Additionally, we define the shorthand $s = \sin\theta_{AB}$ and the effective strength of the Anderson impurity, $f = \alpha_0 v/R\epsilon_o$.

We now consider the case of a strong potential impurity, $u \gg 1$ and a weak Anderson impurity, $f\mathcal{L}_1 \ll 1$. The latter condition implies that the localized level ϵ_o is lying not too close to the Dirac point, on the scale of the energy v/R. For large u, as it turns out, only small values of x are important, where $K_1(x) \sim 1/x$. This simplifies Eq. (56) to the following expression:

$$J_{\text{eff}}^{AB}(\mathbf{R}) = \frac{J^2 s^2 A_o^2}{\pi^3 v R^3}\int_{-\infty}^{\infty} \frac{dx}{(1 + iux\mathcal{L} + fus^2)^2}. \quad (57)$$

Importantly, even though the logarithm $\mathcal{L} = \ln\frac{R}{a|x|}$ is a slow function of x, approximating it with a constant would lead to a zero value of the integral since the two poles of the integrand reside on the same side of the x axis. The nonzero contribution to J_{eff}^{AB} arises from the variation of $\mathcal{L}$. The method of calculating such corrections is explained in Appendix C. Using this method, we find

$$J_{\text{eff}}^{AB}(\mathbf{R}) = -\frac{J^2 A_o \sin^2\theta_{AB}}{\pi U R^2 \left|1 + \frac{\alpha_0 U A_0}{\pi R^2 \epsilon_o}\sin^2\theta_{AB}\right| \mathcal{L}^2(R)}, \quad (58)$$

where the logarithm assumes the value

$$\mathcal{L}(R) = \ln\frac{|U|A_o}{\pi a v} - \ln\left|1 + \frac{\alpha_0 U A_0}{\pi R^2\epsilon_o}\sin^2\theta_{AB}\right|. \quad (59)$$

We see that the two impurities, a strong potential impurity and a weak Anderson impurity, are always ferromagnetically coupled independent of the location of the resonant energy level with respect to the Dirac point. The transition from strong potential impurity to weak impurity limit occurs at $R \sim UA_0/\pi v$, where the integral in Eq. (57) converges over $x \sim 1$ and we get the usual $1/R^3$ dependence, similar to two identical weak impurities, antiferromagnetically coupled.

Figure 11 illustrates the dependence of the spin-exchange coupling J_{AB} on the distance between the impurities for on-site energy $\epsilon_o = 0.5$ eV, $\gamma = 0.1$ eV, and on-site potential, $U = 100$ eV. For these values and range of distances shown in the

plot, the potential impurity is strong while Anderson impurity is weak. The impurities are ferromagnetically coupled as given by Eq. (58).

VI. SUMMARY

Two singly occupied Anderson impurities with the energy level below the Fermi energy interact resonantly with each other. The interaction is facilitated by the exchange of virtual electron-hole excitations. The sign and nature of the interaction depend on whether the impurities reside on the same sublattice or then opposite sublattices.

For opposite sublattices, both the potential part of the interaction and the effective spin-exchange coupling have resonant character when one of the energy levels of the two-impurity system passes through the Dirac points. The potential interaction is repulsive and decays with the third power of the distance R in the weak coupling limit. The resonant potential interaction decays as the first power of the distance and is attractive. The spin-exchange part of the interaction is antiferromagnetic both at small and large distances. At the distances where level crosses the Dirac points, the coupling is ferromagnetic and resonantly enhanced.

For the same sublattice, the potential part of the interaction is attractive in the weak coupling limit and repulsive in the strong coupling limit. The spin-exchange coupling is ferromagnetic at large and small distances but reverses sign and becomes antiferromagnetic for intermediate distances.

In the presence of different types of impurities or defects on graphene, understanding the nature of the interaction between them becomes important as well. The presence of a hydrogen atom along with the vacancy defect can be viewed as the interaction between an Anderson and a substitutional impurity with large on-site potential. In such case, where we have a weak Anderson impurity and a strong potential impurity, both the potential part of the interaction and the spin-spin-exchange coupling behave as $1/R^2$ and are attractive in nature. This result is different from those for two Anderson or two substitutional impurities.

ACKNOWLEDGMENTS

We thank Oleg Starykh for helpful discussions. The work was supported by the Department of Energy, Office of Basic Energy Sciences, Grant No. DE-FG02-06ER46313.

APPENDIX A: CALCULATION OF INTEGRALS INVOLVING SPECIAL FUNCTIONS

(i) The integral in Eq. (24) is of the form

$$I(\beta) = -\int_{-\infty}^{\infty} dx \frac{x^2 K_1^2(|x|)}{(x+i\beta)^2} = -2\int_0^{\infty} dx \frac{x^2 K_1^2(x)(x^2-\beta^2)}{(x^2+\beta^2)^2}. \tag{A1}$$

Integrating by parts and separating the leading contribution to the integral then gives

$$I(\beta) = \frac{\pi^2}{2} + 4\beta^2 \int_0^{\infty} dx \frac{K_1(x)}{(x^2+\beta^2)} \frac{d}{dx}[xK_1(x]. \tag{A2}$$

The main contribution to the remaining integral comes from $x \ll 1$, where we can expand $K_1(x)$ up to second order $x^2K_1^2(x) \approx 1 + x^2\ln(0.54x)/2$ and differentiate it to rewrite the integral as

$$I(\beta) = \frac{\pi^2}{2} + 4\beta^2 \int_0^{\infty} dx \frac{\ln(0.89x)}{(x^2+\beta^2)} = \frac{\pi^2}{2} + 2\pi\beta \ln(0.89\beta). \tag{A3}$$

(ii) The integral in Eq. (30) can also be calculated in a similar way. On integration by parts we get

$$I(\beta) = \int_{-\infty}^{\infty} dx \frac{x^2 K_0^2(|x|)}{(x+i\beta)^2} \approx 4\int_0^{\infty} dx \frac{x^2 K_0(x)}{(x^2+\beta^2)} \frac{d}{dx}[xK_0(x)]. \tag{A4}$$

Using $d(xK_0(x))/dx = K_0(x) - xK_1(x)$ and separating leading contribution to the integral gives

$$I(\beta) = \frac{\pi^2}{2} - 4\beta^2 \int_0^{\infty} dx \frac{K_0^2(x)}{(x^2+\beta^2)} + 4\beta^2 \int_0^{\infty} dx \frac{xK_0(x)K_1(x)}{(x^2+\beta^2)}. \tag{A5}$$

The remaining integrals are easy to calculate by noting that only $x \sim \beta$ are important to the integral and hence for small ϵ we can approximate $K_0(x) \approx -\ln x$ and $K_1(x) \approx 1/x$ to get

$$I(\beta) = \frac{\pi^2}{2} - \frac{\pi^3\beta}{2} - 2\pi\beta\ln^2\beta - 2\pi\beta\ln\beta. \tag{A6}$$

APPENDIX B: CALCULATION OF RESONANT INTEGRAL

To calculate the integral in Eq. (39) near resonance, i.e., for small values of $\rho - \rho_o$ keep terms of lowest order in x. This is justified by the fact that the most important contribution to the integral comes from small arguments $x \ll 1$. Denoting now $\xi = \rho^2 - \rho_0^2$, in the leading logarithmic approximation,

$$\int_{-\infty}^{\infty} \frac{dx(\frac{ixv}{R} - \epsilon_o)^4}{\left(\xi - 2i\rho_0 x\left(\ln\left(\frac{cR}{a|x|}\right)\right)^2\right.} = -\epsilon_o^4 \frac{\partial}{\partial\xi}\int_0^{\infty} \frac{2\xi\, dx}{\xi^2 + 4\rho_0^2 x^2 \ln^2\left(\frac{cR}{a|x|}\right)} = -\epsilon_o^4 \frac{\pi}{2\rho_0|\xi|\ln^2\left(\frac{cR}{a|\xi|}.\right)}, \tag{B1}$$

where c is introduced as $\ln c = \frac{1}{\alpha_0}$. In calculating the above integral, we have made use of the approximation that $\frac{\xi v}{\rho_o \ln(\frac{cR}{a|\xi|})R} \ll \epsilon_o$, thus neglecting xv/R term in the first line in the numerator of Eq. (B1).

APPENDIX C: CALCULATION OF LOGARITHMIC INTEGRALS

To calculate the integral in Eq. (44) for $\rho \ll 1$, we rewrite the spin-exchange coupling in the following form:

$$J_{\text{eff}}^{AA}(\mathbf{R}) = -\frac{J^2}{\pi^3}\frac{A_o^2}{vR^3}\left(\frac{\epsilon_o R}{\alpha_0 v}\right)^3 \int_{-\infty}^{\infty} dz c^2 z^2 \ln^2(B/|z|) \times \frac{1}{\left[\left\{1 + iz\ln\left(\frac{c_1 A}{|z|}\right)\right\}^2 + c^2 z^2 \ln^2\left(\frac{B}{|z|}\right)\right]^2}, \tag{C1}$$

where we have rescaled the integration variable, $x = \rho z$ and introduced the shorthands $A = R/(a\rho)$, $B = 1/\rho$, $c = |\cos\theta_{AA}|$, and $\ln c_1 = \frac{1}{\alpha_0}$. The above integral converges at $z \sim 1$, where we can expand the integrand up to first order in $\ln z$ to get

$$I = \frac{c}{2}\frac{\partial}{\partial c}\int_{-\infty}^{\infty} \frac{dz}{\left[\left\{1 + iz\ln\left(\frac{c_1 A}{|z|}\right)\right\}^2 + c^2 z^2 \ln^2\left(\frac{B}{|z|}\right)\right]}$$
$$= c\frac{\partial}{\partial c}\int_{-\infty}^{\infty} dz \ln|z| \frac{iz(1 + iz\ln c_1 A) + c^2 z^2 \ln B}{[(1 + iz\ln c_1 A)^2 + c^2 z^2 \ln^2 B]^2}. \quad \text{(C2)}$$

The above integral is of the form $\int_{-\infty}^{\infty} dz \ln|z| K(z)$, where $K(z)$ is a rational function with all its singularities located in the upper half-plane of complex z. Defining a new function $Q(z)$ according to $Q(z) = \int_{-\infty}^{z} dz K(z)$, one can use the integration by parts to obtain

$$\int_{-\infty}^{\infty} dz \ln|z| \frac{dQ(z)}{dz} = -P\int_{-\infty}^{\infty} dz \frac{Q(z)}{z}$$
$$= i\pi Q(0) = i\pi \int_{-\infty}^{0} dz K(z). \quad \text{(C3)}$$

In performing this transformation, we have used that $Q(\infty) = \int_{-\infty}^{\infty} dz K(z) = 0$ since the function $K(z)$ does not have any singularities in the lower half-plane of z. Additionally, to express the principal value integral in Eq. (C3) via $Q(0)$, we observe that

$$\int_{-\infty}^{\infty} dz \frac{Q(z)}{z - i0} = P\int_{-\infty}^{\infty} dz \frac{Q(z)}{z} + i\pi Q(0) = 0, \quad \text{(C4)}$$

as the integral in the left-hand side of Eq. (C4) is zero for the already familiar reason: All its poles reside in the upper half-plane. From Eq. (C3), we obtain that the exchange coupling constant Eq. (C2) is expressed in terms of the following integral of a rational function:

$$I = i\pi c\frac{\partial}{\partial c}\int_{-\infty}^{0} dz \frac{iz(1 + iz\ln c_1 A) + c^2 z^2 \ln B}{[(1 + iz\ln c_1 A)^2 + c^2 z^2 \ln^2 B]^2}. \quad \text{(C5)}$$

The above integral can be easily calculated to get

$$I = \frac{\pi}{4c\ln^2 B}\left[\frac{4c^3 \ln(c_1 A/B)\ln^3 B}{(\ln^2 c_1 A - c^2\ln^2 B)^2}\right.$$
$$\left. - \frac{2c\ln c_1 A \ln B}{\ln^2 c_1 A - c^2 \ln^2 B} + \ln\left(\frac{\ln c_1 A + c\ln B}{\ln c_1 A - c\ln B}\right)\right]. \quad \text{(C6)}$$

[1] P. O. Lehtinen, A. S. Foster, Y. C. Ma, A. V. Krasheninnikov, and R. M. Nieminen, Phys. Rev. Lett. **93**, 187202 (2004).
[2] V. M. Pereira, F. Guinea, J. M. B. Lopes dos Santos, N. M. R. Peres, and A. H. Castro Neto, Phys. Rev. Lett. **96**, 036801 (2006).
[3] O. V. Yazyev and L. Helm, Phys. Rev. B **75**, 125408 (2007).
[4] O. V. Yazyev, Rep. Prog. Phys. **73**, 056501 (2010).
[5] V. W. Brar, R. Decker, H.-M. Solowan, Y. Wang, L. Maserati, K. T. Chan, H. Lee, Ç. O. Girit, A. Zettl, S. G. Louie, M. L. Cohen, and M. F. Crommie, Nat. Phys. **7**, 43 (2011).
[6] E. J. G. Santos, A. Ayuela, and D. Sanchez-Portal, New J. Phys. **14**, 043022 (2012).
[7] T. Eelbo, M. Waśniowska, M. Gyamfi, S. Forti, U. Starke, and R. Wiesendanger, Phys. Rev. B **87**, 205443 (2013).
[8] T. Eelbo, M. Waśniowska, P. Thakur, M. Gyamfi, B. Sachs, T. O. Wehling, S. Forti, U. Starke, C. Tieg, A. I. Lichtenstein, and R. Wiesendanger, Phys. Rev. Lett. **110**, 136804 (2013).
[9] M. Gyamfi, T. Eelbo, M. Waśniowska, and R. Wiesendanger, Phys. Rev. B **84**, 113403 (2011).
[10] B. Fischer and M. W. Klein, Phys. Rev. B **11**, 2025 (1975).
[11] M. T. Béal-Monod, Phys. Rev. B **36**, 8835 (1987).
[12] A. H. Castro Neto, F. Guinea, N. M. R. Peres, K. S. Novoselov, and A. K. Geim, Rev. Mod. Phys. **81**, 109 (2009)
[13] A. Bostwick, J. L. McChesney, K. V. Emtsev, T. Seyller, K. Horn, S. D. Kevan, and E. Rotenberg, Phys. Rev. Lett. **103**, 056404 (2009).
[14] D. C. Elias, R. R. Nair, T. M. G. Mohiuddin, S. V. Morozov, P. Blake, M. P. Halsall, A. C. Ferrari, D. W. Boukhvalov, M. I. Katsnelson, A. K. Geim, and K. S. Novoselov, Science **323**, 610 (2009).
[15] R. Balog, B. Jørgensen, L. Nilsson, M. Andersen, E. Rienks, M. Bianchi, M. Fanetti, E. Lægsgaard, A. Baraldi, S. Lizzit, Z. Sljivancanin, F. Besenbacher, B. Hammer, T. G. Pedersen, P. Hofmann, and L. Hornek, Nature (London) **9**, 315 (2010).
[16] J. Ding, Zh. Qiao, W. Feng, Y. Yao, and Q. Niu, Phys. Rev. B **84**, 195444 (2011).
[17] V. V. Mkhitaryan and E. G. Mishchenko, Phys. Rev. B **86**, 115442 (2012).
[18] L. Brey, H. A. Fertig, and S. Das Sarma, Phys. Rev. Lett. **99**, 116802 (2007).
[19] A. M. Black-Schaffer, Phys. Rev. B **81**, 205416 (2010).
[20] I. C. Gerber, A. V. Krasheninnikov, A. S. Foster, and R. M. Nieminen, New J. Phys. **12**, 113021 (2010).
[21] M. Sherafati and S. Satpathy, Phys. Rev. B **83**, 165425 (2011).
[22] E. Kogan, Phys. Rev. B **84**, 115119 (2011).
[23] S. R. Power and M. S. Ferreira, Crystals **3**, 49 (2013).
[24] A. Allerdt, A. E. Feiguin, and S. Das Sarma, Phys. Rev. B **95**, 104402 (2017).
[25] S. Saremi, Phys. Rev. B **76**, 184430 (2007).
[26] B.-L. Huang and C.-Y. Mou, Europhys. Lett. **88**, 68005 (2009).
[27] J. Simonin, Phys. Rev. B **73**, 155102 (2006).
[28] J. E. Bunder and H.-H. Lin, Phys. Rev. B **80**, 153414 (2009).
[29] T. O. Wehling, M. I. Katsnelson, and A. I. Lichtenstein, Chem. Phys. Lett. **476**, 125 (2009).
[30] H. González-Herrero, J. M. Gómez-Rodriguez, P. Mallet, M. Moaied, J. J. Palacios, C. Salgado, M. M. Ugeda, J.-Y. Veuillen, F. Ynduráin, and I. Brihuega, Science **352**, 437 (2016).
[31] I. V. Krainov, I. V. Rozhansky, N. S. Averkiev, and E. Lähderanta, Phys. Rev. B **92**, 155432 (2015).

[32] V. V. Cheianov, O. Syljuasen, B. L. Altshuler, and V. I. Falko, Europhys. Lett. **89**, 56003 (2010).

[33] D. A. Abanin, A. V. Shytov, and L. S. Levitov, Phys. Rev. Lett. **105**, 086802 (2010).

[34] S. Kopylov, V. Cheianov, B. L. Altshuler, and V. I. Fal'ko, Phys. Rev. B **83**, 201401(R) (2011).

[35] A. V. Shytov, D. A. Abanin, and L. S. Levitov, Phys. Rev. Lett. **103**, 016806 (2009).

[36] S. LeBohec, J. Talbot, and E. G. Mishchenko, Phys. Rev. B **89**, 045433 (2014).

[37] M. Agarwal and E. G. Mishchenko, Phys. Rev. B **95**, 075411 (2017).